
A Kernel Framework for PDE Discovery and Operator Learning

Da Long¹ Nicole Mrvaljević² Shandian Zhe¹ Bamdad Hosseini²

Abstract

This article presents a three-step framework for learning and solving partial differential equations (PDEs) using kernel methods. Given a training set consisting of pairs of noisy PDE solutions and source/boundary terms on a mesh, kernel smoothing is utilized to denoise the data and approximate derivatives of the solution. This information is then used in a kernel regression model to learn the algebraic form of the PDE. The learned PDE is then used within a kernel based solver to approximate the solution of the PDE with a new source/boundary term, thereby constituting an operator learning framework. Numerical experiments compare the method to state-of-the-art algorithms and demonstrate its competitive performance.

under previously unseen conditions. The goal of this paper is to present an example of such a workflow based on recent advances in the theory of kernel methods that is robust to noise and supported by theoretical analysis.

To be precise, we consider the setting where the solution of a PDE subject to known forcing is observed at a finite set of locations. This solution is further corrupted by noise and constitutes the training data. Then we consider two problems: (a) *Discover the PDE*, i.e., find the functional relationship between the partial derivatives of the solution that describes the PDE; (b) *Solve the PDE* subject to previously unseen forcing. Problem (a) is often referred to as *equation discovery* and goes back, at least, to the seminal works (Bongard & Lipson, 2007; Schmidt & Lipson, 2009). More recently, it is often tackled by the Sparse Identification of nonlinear Dynamical Systems (SINDy) algorithm of (Brunton et al., 2016) and its subvariants. Problem (b) is classical in the field of applied mathematics and numerical PDEs. However, classical numerical methods are very intrusive and are often tailored to specific types of PDEs. Recent techniques such as the Physics Informed Neural Networks (PINNs) of (Raissi et al., 2019) or the kernel approach of (Chen et al., 2021) can circumvent this issue by relaxing the PDE from an equality constraint to a regression misfit term. Solving Problems (a) and (b) in conjunction yields an *operator learning* framework, where one aims to learn/approximate the infinite-dimensional solution operator of a PDE; the DeepONet algorithm of (Lu et al., 2021) and the Fourier Neural Operator (FNO) approach of (Li et al., 2020b) are state of the art in this context.

1. INTRODUCTION

Partial differential equations (PDEs) are ubiquitous in natural sciences such as physics (Riley et al., 1999), social sciences (Black & Scholes, 1973), biology (Edelstein-Keshet, 2005) and engineering (Marsden & Hughes, 1994; Temam, 2001). To some extent, PDEs are the main subject of interest in the field of Physics Informed Learning (PIL); see (Karniadakis et al., 2021; Carleo et al., 2019; Willard et al., 2020). Traditionally, PDEs are designed or discovered by experts based on mathematical and physical intuition, a process that relies on human expertise, data, and mathematical analysis. Once the PDE is accepted as a model it is often solved using computer algorithms to simulate a real-world process of interest.

Recent advances in machine learning (ML) along with the abundance of data have led to the idea of automating this workflow, thereby promising computer programs for discovering a PDE from limited and noisy data and solving the discovered PDE to predict the state of a physical system

The main contributions of the article are two-fold:

- (1) We present a three-step kernel method for the discovery of PDEs and learning of their solution operators from noisy and limited data: Step (i), kernel smoothing is utilized to denoise the training data and compute pertinent partial derivatives of the solution; Step (ii), kernel regression is used to learn the algebraic form of the PDE; Step (iii), the kernel solver of (Chen et al., 2021) is used to numerically approximate the solution to the discovered PDE under new forcing data.

Step (i) allows us to accommodate input data that are provided on unstructured and inconsistent grids. Step (ii) allows us to learn the functional form of PDEs with

¹School of Computing, University of Utah, UT, USA
²Department of Applied Mathematics, University of Washington, WA, USA. Correspondence to: Bamdad Hosseini <bamdadh@uw.edu>.

variable (spatially or temporally) parameters. Step (iii) is, at the level of implementation, blind to the functional form of the PDE. All three steps inherit the desirable robustness and stability properties of kernel methods and are amenable to kernel learning strategies such as cross validation or kernel flow (Owhadi & Yoo, 2019).

- (2) Our three-step approach is compatible with, and complements, existing PDE discovery algorithms and PDE solvers. For example, the kernel smoothing approach of Step (i) can be used for denoising and gradient estimation within the SINDy and PDE-FIND algorithms of (Rudy et al., 2017), thereby extending these methods to training data given on unstructured grids. In fact, we demonstrate that SINDy can be used in place of our kernel PDE discovery approach in step (ii). At the same time other meshless PDE solvers such as PINNs can replace the one we use in step (iii).

The rest of the article is organized as follows: Section 2 reviews background material; Section 3 outlines our proposed methodology in detail as well as some supporting theory; Section 4 presents our numerical experiments; Section 5 presents a more detailed discussion of our findings and their implementation as well as how our methodology relates to existing methods in the literature; and Section 6 summarizes our conclusions. A detailed review of the relevant literature is presented in Section A followed by implementation details and additional experimental results in Section B.

2. PRELIMINARIES

We collect here some preliminary results and notation that will be used in the remainder of the article.

2.1. Nonlinear PDEs

Suppose $D \geq 1$ and let $\Omega \subset \mathbb{R}^D$ be a compact and simply-connected domain with boundary $\partial\Omega$. Consider the multi-index $\alpha = (\alpha_1, \dots, \alpha_D) \in \mathbb{N}^D$ (i.e., a d -dimensional vector of non-negative integers)¹. Now for a smooth function $u : \Omega \rightarrow \mathbb{R}$ we define the partial derivatives $\partial^\alpha u := \partial_{x_1}^{\alpha_1} \partial_{x_2}^{\alpha_2} \dots \partial_{x_D}^{\alpha_D} u$. We further consider two collections of multi-indices $\{\alpha^1, \dots, \alpha^P\} \subset \mathbb{N}^D$ and $\{\beta^1, \dots, \beta^B\} \subset \mathbb{N}^B$ for integers $P, B \geq 0$. Finally we define $M_P := \max_{1 \leq i \leq P} \|\alpha^i\|_1$ and $M_B := \max_{1 \leq i \leq B} \|\beta^i\|_1$. Throughout the article we have in mind PDEs of the form

$$\mathcal{P}(\mathbf{x}, \partial^{\alpha^1} u(\mathbf{x}), \dots, \partial^{\alpha^P} u(\mathbf{x})) = f(\mathbf{x}), \quad \mathbf{x} \in \Omega, \quad (1a)$$

$$\mathcal{B}(\mathbf{x}, \partial^{\beta^1} u(\mathbf{x}), \dots, \partial^{\beta^B} u(\mathbf{x})) = g(\mathbf{x}), \quad \mathbf{x} \in \partial\Omega, \quad (1b)$$

¹Henceforth we use bold letters to denote d -dimensional vectors of integers or reals for $d \geq 2$.

where $\mathcal{P} : \mathbb{R}^{J_P} \rightarrow \mathbb{R}$ and $\mathcal{B} : \mathbb{R}^{J_B} \rightarrow \mathbb{R}$, with $J_P = D + P$ and $J_B = D + B$, are nonlinear functions that define the functional relationships between $\mathbf{x} = (x_1, \dots, x_D)$ and values of u and its partial derivatives in the interior and boundary of Ω . The functions $f : \Omega \rightarrow \mathbb{R}$, often referred to as a forcing/source term, and $g : \partial\Omega \rightarrow \mathbb{R}$, the boundary condition, constitute the data of the PDE. In most practical problems, $M_B \leq M_P$ and $\max\{M_P, M_B\}$ denotes the *order* of the PDE. As a running example consider the one-dimensional second order PDE

$$-\partial_x [a(x)\partial_x u(x)] + u^3(x) = f(x), \quad x \in (0, 1), \quad (2)$$

$$u(0) = u(1) = 0,$$

where $a \in C^1(\overline{\Omega})$ is a spatially varying coefficient, for example, drawn from a random field. We assume this coefficient along with its first derivative can be evaluated but in general it may have a complicated or unknown form. We can readily read that $\mathcal{B}(x, u(x)) \equiv u(x)$. Expanding the differential operator on the left hand side of the PDE we get $\mathcal{P}(x, u(x), \partial_x u(x), \partial_x^2 u(x)) = -\partial_x a(x)\partial_x u(x) - a(x)\partial_x^2 u(x) + u^3(x)$. Thus, defining the new variables² $\mathbf{s} = (s_1, \dots, s_4) \equiv [x, u(x), u_x(x), u_{xx}(x)] \in \mathbb{R}^4$ and $\mathbf{t} = (t_1, t_2) \equiv [x, u(x)] \in \mathbb{R}^2$ we can write

$$\mathcal{P}(\mathbf{s}) = -a_x(s_1)s_3 - a(s_1)s_4 + s_2^3,$$

$$\mathcal{B}(\mathbf{t}) = t_2.$$

Throughout the rest of the article we will assume that whenever a PDE is presented, it is well-defined and has a unique strong solution u , i.e., a solution that is defined pointwise.

2.2. Representer Theorems

Consider a simply connected set $\Theta \subseteq \mathbb{R}^D$. Following (Muandet et al., 2017), we say that a function $\mathcal{K} : \Theta \times \Theta \rightarrow \mathbb{R}$ is a *Mercer kernel* if it is symmetric, that is $\mathcal{K}(\mathbf{s}_1, \mathbf{s}_2) = \mathcal{K}(\mathbf{s}_2, \mathbf{s}_1)$, and that for any collection of points $S = \{\mathbf{s}_1, \dots, \mathbf{s}_n\}$ the matrix $[\mathcal{K}(S, S)]_{ij} = \mathcal{K}(\mathbf{s}_i, \mathbf{s}_j)$ is positive definite. We write $\mathcal{H}_{\mathcal{K}}$ to denote the Reproducing Kernel Hilbert Space (RKHS) associated to \mathcal{K} with its norm denoted by $\|\cdot\|_{\mathcal{K}}$.

Suppose $\mathcal{H}_{\mathcal{K}}$ is continuously embedded in $C^k(\Theta)$, the Banach space of real valued functions that are k -times continuously differentiable with $k \in \mathbb{N}$ equipped with the usual sup norm, and fix the points $X = \{\mathbf{x}_1, \dots, \mathbf{x}_J\} \subset \Theta$. Let $\delta_j : C^0(\Theta) \rightarrow \mathbb{R}$ denote the pointwise evaluation operator mapping a function $u \in C^0(\Theta)$ to its point value $u(\mathbf{x}_j)$ for $(1 \leq j \leq J)$, let $L_q : C^k(\Theta) \rightarrow C^0(\Theta)$ for $q = 1, \dots, Q$ be bounded and linear operators, and define the maps

$$\phi_j^q := \delta_j \circ L_q, \quad u \mapsto L_q(u)(\mathbf{x}_j),$$

²The entries s_i, t_i simply denote the values of x as well as u and its partial derivatives evaluated at x . This compact notation will be useful later on.

which first apply the L_q operators to a regular function u and then evaluate the output at the point \mathbf{x}_j . For the PDE solver of (Chen et al., 2021), these maps often evaluate u or some of its partial derivatives at a set of collocation points. Concatenating the ϕ_j^q along the j and q indices we obtain a vector of maps $\phi : C^\alpha(\Theta) \rightarrow \mathbb{R}^N$, where $N = QJ$. The ordering of the ϕ_j^q is innocuous and henceforth we write ϕ_n for $n = 1, \dots, N$ to denote the entries of the vector ϕ .

We now consider optimal recovery problems of the form

$$\underset{u \in \mathcal{H}_{\mathcal{K}}}{\text{minimize}} \|u\|_{\mathcal{K}} \quad \text{s.t.} \quad \phi(u) = \mathbf{o}, \quad (3)$$

where $\mathbf{o} \in \mathbb{R}^N$ is a fixed vector. It is well-known (see for example Chapter 12 of (Owhadi & Scovel, 2019)) that the minimizer \bar{u} of this optimization problem has the form

$$\bar{u}(\mathbf{x}) = \mathcal{K}(\mathbf{x}, \phi) \mathcal{K}(\phi, \phi)^{-1} \mathbf{o}. \quad (4)$$

Here $\mathcal{K}(\mathbf{x}, \phi)$ is a vector field on Θ with entries $[\mathcal{K}(\mathbf{x}, \phi)]_i = \phi_i(\mathcal{K}(\mathbf{x}, \cdot))$ for $i = 1, \dots, N$ and $\mathcal{K}(\phi, \phi) \in \mathbb{R}^{N \times N}$ is a symmetric matrix with entries $[\mathcal{K}(\phi, \phi)]_{ij} = \phi_i \otimes \phi_j(\mathcal{K})$, i.e., we apply ϕ_i along the first argument of \mathcal{K} then apply ϕ_j along the second argument.

One can also extend this formula to nonlinear regression problems of the form

$$\underset{u \in \mathcal{H}_{\mathcal{K}}}{\text{minimize}} \|u\|_{\mathcal{K}}^2 + \frac{1}{\lambda^2} \|\mathcal{F} \circ \phi(u) - \mathbf{o}\|_2^2, \quad (5)$$

where $\lambda > 0$ determines regularization strength, $\mathcal{F} : \mathbb{R}^N \rightarrow \mathbb{R}^O$ is a nonlinear map, and $\mathbf{o} \in \mathbb{R}^O$. By Proposition 2.3 of (Chen et al., 2021), minimizers \bar{u} of (5) have the form

$$\bar{u}(\mathbf{x}) = \mathcal{K}(\mathbf{x}, \phi) \mathcal{K}(\phi, \phi)^{-1} \bar{\mathbf{z}}, \quad (6)$$

where the vector $\bar{\mathbf{z}}$ solves the optimization problem

$$\underset{\mathbf{z} \in \mathbb{R}^N}{\text{minimize}} \mathbf{z}^T \mathcal{K}(\phi, \phi)^{-1} \mathbf{z} + \frac{1}{\lambda^2} \|\mathcal{F}(\mathbf{z}) - \mathbf{o}\|_2^2. \quad (7)$$

In the special case where $N = O$ and $\mathcal{F} = \text{Id}$ we obtain

$$\bar{u}(\mathbf{x}) = \mathcal{K}(\mathbf{x}, \phi) (\mathcal{K}(\phi, \phi) + \lambda^2 I)^{-1} \mathbf{o}, \quad (8)$$

by analytically solving (7) and substituting in (6).

During the smoothing of data and PDE discovery steps of our approach we simply take $\mathcal{F} = \text{Id}$. When solving nonlinear PDEs it is often the case that $O < N$ and \mathcal{F} turns out to be a nonlinear map defined via the functional form of the PDE, i.e., the functions \mathcal{P}, \mathcal{B} in (1) and so the second term in (5) measures the residual of the PDE at the collocation points (see (Chen et al., 2021) for more details).

3. METHODOLOGY

We now outline our kernel methodology for equation discovery and operator learning of PDEs from empirical data. We first present an abstract three-step framework for equation discovery and operator learning after which we outline our kernel approach for each single step. For simplicity we will only consider the case where the function \mathcal{P} in (1) is unknown since this is most practically relevant. The approach can be extended to learn \mathcal{B} in a similar manner. We will also assume that the order $M_{\mathcal{P}}$ of the PDE is known.

3.1. An Abstract Framework for Equation Discovery and Operator Learning

Suppose a set of mesh/observation points $X = \{\mathbf{x}_j\}_{j=1}^J \subset \Omega$ is fixed and let $\{u^{(i)}, f^{(i)}\}_{i=1}^I$ be pairs of solutions and forcing terms for the PDE (1) with the same boundary conditions. Our training data consists of noisy observations of the pairs $(u^{(i)}, f^{(i)})$ at the points X , that is,

$$\begin{aligned} \mathbb{R}^J \ni \mathbf{u}^{(i)} &= u^{(i)}(X) + \boldsymbol{\epsilon}^{(i)}, \\ \mathbb{R}^J \ni \mathbf{f}^{(i)} &= f^{(i)}(X), \end{aligned}$$

where we used the shorthand notation $u(X) = (u(\mathbf{x}_1), \dots, u(\mathbf{x}_J))$ and $\boldsymbol{\epsilon}^{(i)} \sim N(0, \lambda_{\mathcal{U}}^2 I)$ is the measurement noise with standard deviation $\lambda_{\mathcal{U}} > 0$. Given this input/training data we then consider a three-step framework:

Step (i): Smoothing the Training Data and Estimating Derivatives. Consider a Banach space \mathcal{H} that is continuously embedded in $C^{M_{\mathcal{P}}}(\Omega)$. Then solve the regression problems

$$\bar{u}^{(i)} = \arg \min_{v \in \mathcal{H}} \|v\|_{\mathcal{H}}^r + \frac{1}{\lambda_{\mathcal{U}}^2} \|v(X) - \mathbf{u}^{(i)}\|_2^2 \quad (9)$$

for $i = 1, \dots, I$ and $r > 0$. Proceed to compute the partial derivatives $\partial^{\alpha_j} \bar{u}^{(i)}(X)$ for $j = 1, \dots, P$, i.e., the pertinent partial derivatives of the smoothed solutions involved in (1) evaluated at the mesh points X ³.

Step (ii): Learning the Functional Form of the PDE. Define the set of vectors

$$\bar{\mathbf{s}}_j^{(i)} = (\mathbf{x}_j, \partial^{\alpha_1} \bar{u}^{(i)}(\mathbf{x}_j), \dots, \partial^{\alpha_P} \bar{u}^{(i)}(\mathbf{x}_j)) \in \mathbb{R}^{J_P}, \quad (10)$$

for $i = 1, \dots, I$. Now consider another Banach space \mathcal{H}' that is continuously embedded in $C^0(\mathbb{R}^{J_P})$ and approximate the function \mathcal{P} via the optimal recovery problem⁴

$$\bar{\mathcal{P}} = \arg \min_{\mathcal{V} \in \mathcal{H}'} \|\mathcal{V}\|_{\mathcal{H}'} \quad \text{s.t.} \quad \mathcal{V}(\bar{\mathbf{s}}_j^{(i)}) = f^{(i)}(\mathbf{x}_j), \quad (11)$$

³If one wishes to learn the boundary operator \mathcal{B} then the $\partial^{\beta_j} \bar{u}^{(i)}$ should also be computed at a set of boundary collocation points.

⁴One can also formulate a regression problem analogous to Step (i) if the $f^{(i)}(X)$ are believed to be noisy.

for $i = 1, \dots, I$ and $j = 1, \dots, J$.

Step (iii): Operator Learning by Solving the Learned PDE. Consider a new source term \tilde{f} for which we wish to approximate the solution to the PDE (1). Since \mathcal{P} is unknown formulate the following PDE instead

$$\begin{aligned}\bar{\mathcal{P}}(\mathbf{x}, \partial^{\alpha_1} u(\mathbf{x}), \dots, \partial^{\alpha_P} u(\mathbf{x})) &= \tilde{f}(\mathbf{x}), \mathbf{x} \in \Omega, \\ \mathcal{B}(\mathbf{x}, \partial^{\beta_1} u(\mathbf{x}), \dots, \partial^{\beta_B} u(\mathbf{x})) &= g(\mathbf{x}), \mathbf{x} \in \partial\Omega.\end{aligned}$$

Note that $\bar{\mathcal{P}}$ is the function given by (11) and this PDE is in general not well-posed unless we pose stringent conditions on $\bar{\mathcal{P}}$. Henceforth we think of ‘‘solving’’ this PDE simply by finding a function \tilde{u} that approximately satisfies the equations. To do so, take new sets of collocation points $\{\tilde{\mathbf{x}}_1, \dots, \tilde{\mathbf{x}}_{\tilde{J}_\Omega}\} \subset \Omega$ (the interior points) and $\{\tilde{\mathbf{x}}_{\tilde{J}_\Omega+1}, \dots, \tilde{\mathbf{x}}_{\tilde{J}}\} \subset \partial\Omega$ (the boundary points). Choose parameters $r, \lambda_{\mathcal{P}}, \lambda_{\mathcal{B}} > 0$ and approximate \tilde{u} by solving the optimization problem⁵

$$\begin{aligned}\hat{u} &:= \arg \min_{u \in \mathcal{H}} \|u\|_{\mathcal{H}}^r \\ &+ \frac{1}{\lambda_{\mathcal{P}}^2} \sum_{j=1}^{\tilde{J}_\Omega} |\bar{\mathcal{P}}(\tilde{\mathbf{x}}_j, \partial^{\alpha_1} u(\tilde{\mathbf{x}}_j), \dots, \partial^{\alpha_P} u(\tilde{\mathbf{x}}_j)) - \tilde{f}(\tilde{\mathbf{x}}_j)|^2 \\ &+ \frac{1}{\lambda_{\mathcal{B}}^2} \sum_{j=\tilde{J}_\Omega+1}^{\tilde{J}} |\mathcal{B}(\tilde{\mathbf{x}}_j, \partial^{\beta_1} u(\tilde{\mathbf{x}}_j), \dots, \partial^{\beta_B} u(\tilde{\mathbf{x}}_j)) - g(\tilde{\mathbf{x}}_j)|^2.\end{aligned}\tag{12}$$

3.2. Implementation Using Kernels

In what follows we present a kernel implementation of our three-step framework by choosing the \mathcal{H} and \mathcal{H}' as appropriate RKHSs.

Step (i): Let $\mathcal{U} : \Omega \times \Omega \rightarrow \mathbb{R}$ be a Mercer kernel chosen so that its RKHS $\mathcal{H}_{\mathcal{U}}$ is continuously embedded in $C^{MP}(\Omega)$. A simple choice would be the RBF kernel $\mathcal{U}(\mathbf{x}_1, \mathbf{x}_2) = \exp\left(\frac{-1}{2l^2} \|\mathbf{x}_1 - \mathbf{x}_2\|_2^2\right)$ whose RKHS consists of infinitely smooth functions⁶. Consider the regression problem (9) with $\mathcal{H} \equiv \mathcal{H}_{\mathcal{U}}$ and $r = 2$. We can solve this problem by applying formula (4) with $\phi = (\delta_1, \dots, \delta_J)$ to obtain the minimizer

$$\tilde{u}^{(i)}(\mathbf{x}) = \mathcal{U}(\mathbf{x}, X) (\mathcal{U}(X, X) + \lambda_{\mathcal{U}}^2 I)^{-1} \mathbf{u}^{(i)}.\tag{13}$$

For any multi-index α_j we can directly differentiate this formula to get

$$\partial^{\alpha_j} \tilde{u}^{(i)}(\mathbf{x}) = \partial^{\alpha_j} \mathcal{U}(\mathbf{x}, X) (\mathcal{U}(X, X) + \lambda_{\mathcal{U}}^2 I)^{-1} \mathbf{u}^{(i)},\tag{14}$$

⁵One can take u in a different space than \mathcal{H} if a priori knowledge of its regularity exists.

⁶The RBF kernel may result in overly smoothed training data in which case the Matérn family of kernels (see (Genton, 2001)) may be a better choice as they allow precise control over the regularity of the RKHS.

where we introduced the vector field $[\partial^{\alpha_j} \mathcal{U}(\mathbf{x}, X)]_i = \partial^{\alpha_j} \mathcal{U}(\mathbf{x}, \mathbf{x}_i)$, the entries of which can be computed offline using analytic expressions or automatic differentiation.

Step (ii): With formula (14) at hand we compute the vectors $\tilde{\mathbf{s}}_j^{(i)}$ following (10). We then choose a Mercer kernel $\mathcal{K} : \mathbb{R}^{J_P} \times \mathbb{R}^{J_P} \rightarrow \mathbb{R}$ with RKHS $\mathcal{H}_{\mathcal{K}}$ which is assumed to be continuously embedded in $C^0(\mathbb{R}^{J_P})$; once again the RBF kernel would be a simple choice⁷. We then formulate the optimal recovery problem (11) with $\mathcal{H}' \equiv \mathcal{H}_{\mathcal{K}}$. Then by equation (4) we have an explicit formula for $\bar{\mathcal{P}}$,

$$\bar{\mathcal{P}}(\mathbf{s}) = \mathcal{K}(\mathbf{s}, S) (\mathcal{K}(S, S) + \lambda_{\mathcal{K}}^2 I)^{-1} \mathbf{f},\tag{15}$$

where we introduced an additional nugget parameter $\lambda_{\mathcal{K}} > 0$ to improve the conditioning of the kernel matrix $\mathcal{K}(S, S)$ as is customary in kernel interpolation or regression.

Step (iii): Finally we consider problem (12) and, following (Chen et al., 2021), we take $\mathcal{H} \equiv \mathcal{H}_{\mathcal{U}}$ and $r = 2$. Let $\tilde{\delta}_j$ denote the pointwise evaluation operator at $\tilde{\mathbf{x}}_j$ and define the maps $\tilde{\phi}_j^i = \tilde{\delta}_j \circ \partial^{\alpha_i}$, for $i = 1, \dots, p$ and $j = 1, \dots, \tilde{J}_\Omega$ as well as $\tilde{\psi}_j^i = \tilde{\delta}_j \circ \partial^{\beta_i}$, for $i = 1, \dots, q$ and $j = \tilde{J}_\Omega + 1, \dots, \tilde{J}$. Further define the vector valued operators $\tilde{\phi}_j := (\tilde{\phi}_j^1, \dots, \tilde{\phi}_j^p)$ and $\tilde{\psi}_j := (\tilde{\psi}_j^1, \dots, \tilde{\psi}_j^q)$. We can now rewrite (12) in the compact form

$$\begin{aligned}\text{minimize}_{u \in \mathcal{H}_{\mathcal{K}}} \|u\|_{\mathcal{K}}^2 &+ \frac{1}{\lambda_{\mathcal{P}}^2} \sum_{j=1}^{\tilde{J}_\Omega} \left| \bar{\mathcal{P}}(\tilde{\mathbf{x}}_j, \tilde{\phi}_j(u)) - \tilde{f}(\tilde{\mathbf{x}}_j) \right|^2 \\ &+ \frac{1}{\lambda_{\mathcal{B}}^2} \sum_{j=\tilde{J}_\Omega+1}^{\tilde{J}} \left| \mathcal{B}(\tilde{\mathbf{x}}_j, \tilde{\psi}_j(u)) - g(\tilde{\mathbf{x}}_j) \right|^2.\end{aligned}$$

Realizing that this is precisely the same form as (5) we evoke formula (6) to identify the minimizer \hat{u} as

$$\hat{u}(\mathbf{x}) = \mathcal{K}(\mathbf{x}, \tilde{\phi}) \mathcal{K}(\tilde{\phi}, \tilde{\phi})^{-1} \hat{\mathbf{z}},$$

where we defined $\tilde{\phi} := (\tilde{\phi}_1, \dots, \tilde{\phi}_{\tilde{J}_\Omega}, \tilde{\psi}_{\tilde{J}_\Omega+1}, \dots, \tilde{\psi}_{\tilde{J}})$ and $\hat{\mathbf{z}}$ is the minimizer of the optimization problem

$$\begin{aligned}\text{minimize}_{\mathbf{z}=(\mathbf{z}_1, \dots, \mathbf{z}_{\tilde{J}})} \mathbf{z}^T \mathcal{U}(\tilde{\phi}, \tilde{\phi})^{-1} \mathbf{z}^T &+ \frac{1}{\lambda_{\mathcal{P}}^2} \sum_{j=1}^{\tilde{J}_\Omega} |\bar{\mathcal{P}}(\mathbf{z}_j) - \tilde{f}(\tilde{\mathbf{x}}_j)|^2 \\ &+ \frac{1}{\lambda_{\mathcal{B}}^2} \sum_{j=\tilde{J}_\Omega+1}^{\tilde{J}} |\mathcal{B}(\mathbf{z}_j) - g(\tilde{\mathbf{x}}_j)|^2.\end{aligned}\tag{16}$$

In practice we solve this problem using a gradient descent algorithm, such as the Gauss-Newton algorithm proposed in (Chen et al., 2021) or L-BFGS.

⁷Another possible choice is the polynomial kernel; see Section B

3.3. Theory

We now present a convergence theory for the kernel implementation of Step (i) using classic results from theory of scattered data approximation indicating the desirable convergence properties of our implementation for denoising the training data and estimating the derivatives. Let us consider the idealized analogue of problem (9) where $\epsilon^{(i)} \equiv 0$ leading to the optimal recovery problem

$$\bar{u}^{(i)} = \arg \min_{v \in \mathcal{H}_U} \|v\|_{\mathcal{U}} \quad \text{s.t.} \quad v(X) = \mathbf{u}^{(i)}. \quad (17)$$

Note that $X = \{\mathbf{x}_j\}_{j=1}^J \subset \Omega$. We can then obtain a rate for the convergence of $\bar{u}^{(i)}$ towards $u^{(i)}$ for $i = 1, \dots, I$.

Theorem 3.1. *Suppose Ω is simply connected, bounded, and has a Lipschitz boundary. Consider real numbers k, t such that $k > t > D/2 + M_P$ and suppose \mathcal{H}_U is continuously embedded in the Sobolev space $H^k(\Omega)$ and that $u^{(i)} \in \mathcal{H}_U$. Define the fill-distance $h_{X,\Omega} := \sup_{\mathbf{x}' \in \Omega} \inf_{\mathbf{x} \in X} |\mathbf{x} - \mathbf{x}'|$. Then for sufficiently small $h_{X,\Omega}$ there exists $C > 0$, independent of $u^{(i)}$ and $h_{X,\Omega}$, so that*

$$\|\bar{u}^{(i)} - u^{(i)}\|_{H^t(\Omega)} \leq Ch_{X,\Omega}^{k-t} \|u^{(i)}\|_{\mathcal{H}_U},$$

where the $\bar{u}^{(i)}$ are given by (17).

The proof is a direct application of Proposition 11.30 of (Wendland, 2004) under the assumption that \mathcal{H}_U is embedded in the Sobolev space $H^k(\Omega)$. We also note that the above theorem does not only give a convergence rate for the functions $\bar{u}^{(i)}$ but also for their requisite partial derivatives of order M_P thanks to the Sobolev Embedding theorem (See Chapter 4 of (Adams & Fournier, 2003)) which states that $H^t(\Omega)$ is continuously embedded in $C^{M_P}(\Omega)$ under the hypothesis of Theorem 3.1.

One can also aim to obtain similar results for Steps (ii) and (iii) of our approach using RKHS theory. Doing so is not trivial due to the propagation of errors from each step to the next. This analysis is the subject of the upcoming publications (Batlle et al., 2023; Hosseini et al., 2023).

4. EXPERIMENTS

Below we compare our computational framework to state-of-the-art algorithms for equation discovery and operator learning. Here we focus on presenting the results and give a brief summary of the setup. Further details of experiments can be found in Section B of Appendix.

Three benchmark DEs were considered: a pendulum model (18), a nonlinear diffusion PDE (19), and the Darcy flow PDE (20). For the PDE learning/discovery task we compared our kernel method to SINDy (Rudy et al., 2017) for the pendulum and diffusion PDEs. Both our method and

SINDy were trained using the same training data with our kernel method used to denoise the training solutions $u^{(i)}$ and to compute the relevant partial derivatives. The kernel parameters in this step were tuned using CV. A test data set was then constructed by taking the same training source terms $f^{(i)}$ from the training set, perturbing them in a controlled manner, and solving the DEs using an independent solver. The Darcy flow PDE was excluded from these experiments since it is unclear how to choose a SINDy dictionary for PDEs with spatially variable coefficients.

For operator learning we used our kernel method and SINDy for Steps (i) and (ii) and used the resulting $\bar{\mathcal{P}}$'s coupled with the kernel PDE solver of (Chen et al., 2021) for Step (iii). Results were further compared with the DeepONet algorithm (Lu et al., 2022) (both the original version and the POD-DeepONet) and the Fourier Neural Operator (FNO) method of (Li et al., 2020b), trained using the same training data set, to learn the mapping from the source term f to the solution u . Throughout the experiments we also used a second POD-DeepONet, denoted as POD-DeepONet (L) in our tables, which is a large network that we tuned to maximize performance and achieve the closest results to our kernel method. All operator learning methods were validated on a test set consisting of new pairs of solutions and source terms. Errors were computed via comparison to an independent high-resolution PDE solver that was taken as ground truth.

4.1. Pendulum

The following system of ODEs modeling the motion of a pendulum was considered

$$\begin{aligned} (u_1)_t(t) &= u_2(t), \\ (u_2)_t(t) &= -k \sin(u_1(t)) + f(t), \end{aligned} \quad (18)$$

subject to $u_1(0) = u_2(0) = 0$. Note that here we used the parameter t as our input parameter rather than just x as is common notation in ODE and PDE literature. The training data for this experiment consists of the pairs of solutions and forcing functions $(u^{(i)}(t_j), f^{(i)}(t_j))$ for $i = 1, \dots, I$ (we took $I = 10$ or 20). Each forcing $f^{(i)}$ was drawn from a GP and the points t_j were distributed uniformly; see Section B.

Equation Discovery/Learning: The function $\bar{\mathcal{P}}$ was learned using our kernel approach for Step (ii) as well as SINDy; see Section B.3 for details including the choice of the dictionary. We took $I = 20$ (size of the training set) and for testing, the forcing terms $f^{(i)}$ were perturbed using the formula $f_\beta^{(i)} = f^{(i)}(t) + \beta \sin(5\pi t)$, the parameter β controls size of the perturbation and hence, the departure of the test and training sets. The ODEs were then solved using an independent solver to obtain the perturbed solutions $u_\beta^{(i)}$. The kernel smoothing of Step (i) was then used to estimate the pertinent derivatives of the $u_\beta^{(i)}$ which were then used

to define a new set of inputs over which the error between $\overline{\mathcal{P}}$ and \mathcal{P} was computed for our kernel method and SINDy. The results are reported in Figure 1 where we observe that our approach with \mathcal{K} taken to be the polynomial kernel (see Section B.2 for the definition of our kernels) almost perfectly matches SINDy (the points overlap almost perfectly) and the learned equations are very robust to perturbations of the test set, a sign that $\overline{\mathcal{P}}$ is a good approximation to \mathcal{P} , globally. Taking \mathcal{K} to be the ARD kernel results in different behavior where the error is larger and grows with β , a sign that $\overline{\mathcal{P}}$ locally approximated \mathcal{P} .

Operator Learning: For operator learning we used our method and SINDy to learn $\overline{\mathcal{P}}$ as above with training data of size $I = 10$ and 20 and compared our three-step approach to DeepONets and FNO. The trained models were then validated on a test set of 50 solution-forcing pairs that were generated by the same procedure as the training set. Table 1 compares the average L^2 errors for the operator learning of the pendulum model. We observed that our method with the polynomial kernel is able to achieve the best performance although the errors are close to the ARD kernel and SINDy. The POD-DeepONet (L) model is the next competitive model despite being an order of magnitude worse and using a much larger neural network, i.e., more expensive parameterization.

We also repeated our experiments by adding Gaussian noise to the training data (we used a noise to signal ratio of 0.1), meaning that the solution-forcing terms are no longer satisfying the underlying DE. Results for this experiment are summarized in Table 2. As expected, this additional noise reduces the accuracy of all models but our method using the ARD kernel was still able to achieve the best performance. We note that the SINDy method also had very close performance. FNO achieved the next best result but it was still worse by a factor of 2.

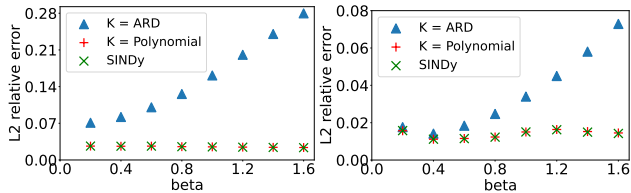


Figure 1. Test error of the learned function $\overline{\mathcal{P}}$ with our method vs. SINDy for the pendulum ODE (left) and the nonlinear diffusion PDE (right). The parameter β controls the departure of the test and training forcing terms. Results for the polynomial kernel overlapped with SINDy.

Method	$I = 10$	$I = 20$
$\mathcal{K} = \text{ARD}$	$7.5e^{-3}$ ($1.4e^{-3}$)	$2.3e^{-3}$ ($3.1e^{-4}$)
$\mathcal{K} = \text{Polynomial}$	$6.3e^{-3}$ ($1.1e^{-3}$)	$2.1e^{-3}$ ($1.7e^{-4}$)
SINDy	$7.1e^{-3}$ ($8.5e^{-4}$)	$4.5e^{-3}$ ($4.5e^{-3}$)
POD-DeepONet	$1.8e^{-1}$ ($2.7e^{-2}$)	$5.7e^{-2}$ ($7.1e^{-3}$)
POD-DeepONet (L)	$3.7e^{-2}$ ($5.3e^{-3}$)	$1.0e^{-2}$ ($1.1e^{-3}$)
FNO	$1.2e^{-1}$ ($1.3e^{-2}$)	$4.1e^{-2}$ ($3.8e^{-3}$)
DeepONet	$2.9e^{-1}$ ($2.8e^{-2}$)	$1.3e^{-1}$ ($1.2e^{-2}$)

Table 1. Average L^2 relative errors for the operator learning task of pendulum system computed for 50 test forcing functions. Standard deviations are reported in brackets. (L) indicates the large network variant of POD-DeepONet. Bold text indicates the best errors.

Method	Pendulum	Diffusion	Darcy Flow
Our method	$3.9e^{-2}$ ($2.3e^{-3}$)	$6.3e^{-2}$ ($4.6e^{-3}$)	$7.7e^{-2}$ ($5.0e^{-3}$)
POD-DeepONet	$9.7e^{-2}$ ($1.3e^{-2}$)	$1.4e^{-1}$ ($1.1e^{-2}$)	$9.8e^{-2}$ ($7.2e^{-3}$)
POD-DeepONet (L)	$8.1e^{-2}$ ($1.0e^{-2}$)	$1.0e^{-1}$ ($8.8e^{-3}$)	$7.2e^{-2}$ ($6.5e^{-3}$)
FNO	$8.0e^{-2}$ ($6.8e^{-3}$)	$7.7e^{-2}$ ($5.0e^{-3}$)	$8.8e^{-2}$ ($9.0e^{-3}$)
DeepONet	$1.5e^{-1}$ ($1.9e^{-2}$)	$2.3e^{-1}$ ($1.8e^{-2}$)	$1.5e^{-1}$ ($1.6e^{-2}$)
SINDy	$4.1e^{-2}$ ($3.8e^{-3}$)	$6.8e^{-2}$ ($2.3e^{-3}$)	N/A

Table 2. Average L^2 relative errors for the operator learning task computed for 50 test forcing functions with 0.1 noise level in the training data. Standard deviations are reported in brackets. For our method, we report the best one from the ARD kernel and the polynomial kernel. (L) indicates the large network variant of POD-DeepONet. Bold text indicates the best errors.

4.2. Nonlinear Diffusion PDE

The following second order nonlinear PDE was considered for our second set of experiments

$$u_t(x, t) = 0.01u_{xx}(x, t) + 0.01u^2(x) + f(x), \quad (19)$$

$$(x, t) \in (0, 1) \times (0, 1],$$

subject to boundary conditions $u(0, t) = u(1, t) = 0$ for $t \in (0, 1]$ and initial conditions $u(x, 0) = 0$, for $x \in (0, 1)$. Similar to Section 4.1, the training data was generated by drawing random sources $f^{(i)}(x)$ from a GP with the RBF kernel; note that f is only a function of x here and hence a one dimensional function. As a benchmark PDE solver in this example we used the same finite-difference solver used by (Lu et al., 2021). For detailed explanation of the setup for this experiment see Section B.4.

Equation Discovery/Learning: We followed the same recipe as the equation discovery experiments from Section 4.1 to compare our kernel approach, with the Gaussian kernel, to SINDy. We trained the model using a training data set of size $I = 20$ and tested the learned $\overline{\mathcal{P}}$ functions on a test set that was obtained via perturbation of the training set, parameterized by the β parameter. The results of our experiments are presented in Figure 1. Here we see a similar picture to the case of the pendulum ODE, i.e., the polynomial kernel matched the performance of SINDy, and yielded a global approximation while the ARD kernel resulted in a local approximant.

Operator Learning: For operator learning experiments we followed the recipe of Section 4.1 once more. All models were trained on data sets of size $I = 10$ and 20 and validated on a test set of size 50, all generated using the same procedure but independently. Table 3 summarizes our results with the exact training data. We observe similar trends as the pendulum example with the polynomial kernel achieving the best errors with SINDy achieving slightly worse performance. Interestingly, in this case the ARD kernel appears to perform significantly worse. Among the neural net methods the large POD-DeepONet was most competitive. We also performed the experiments after adding artificial noise to the training data; the results are presented in Table 2. Once again we found that our method achieved the lowest error, followed closely by SINDy. The FNO was once again the best performing neural net based method.

Method	$I = 10$	$I = 20$
$\mathcal{K} = \text{ARD}$	$1.3e^{-2}(2.1e^{-3})$	$7.5e^{-3}(1.1e^{-3})$
$\mathcal{K} = \text{Polynomial}$	$7.0e^{-3}(5.7e^{-4})$	$4.1e^{-3}(2.4e^{-4})$
POD-DeepONet	$1.7e^{-1}(1.5e^{-2})$	$7.8e^{-2}(6.1e^{-3})$
POD-DeepONet (L)	$4.4e^{-2}(3.6e^{-3})$	$1.4e^{-2}(1.3e^{-3})$
FNO	$5.8e^{-2}(4.1e^{-3})$	$1.6e^{-2}(1.3e^{-3})$
DeepONet	$3.4e^{-1}(1.9e^{-2})$	$1.8e^{-1}(1.5e^{-2})$
SINDy	$9.6e^{-3}(9.3e^{-4})$	$4.2e^{-3}(2.3e^{-4})$

Table 3. Average L^2 relative errors for the operator learning task of diffusion computed for 50 test forcing functions. Standard deviations are reported in brackets. (L) indicates the large network variant of POD-DeepONet. Bold text indicates the best errors.

4.3. Darcy Flow

For our third and final example we considered the Darcy flow PDE

$$-\text{div}(a\nabla u)(x) = f(x), \quad x \in (0, 1)^2, \quad (20)$$

subject to homogeneous Dirichlet boundary conditions. The coefficient a is a spatially variable field given by $a(x) = \exp(\sin(\pi x_1) + \sin(\pi x_2)) + \exp(-\sin(\pi x_1) - \sin(\pi x_2))$. In this experiment we excluded SINDy as the construction of an appropriate dictionary for PDEs with spatially variable coefficients is *not* possible without prior knowledge of the form of the PDE; see Section 5. Therefore, here we focus primarily on the operator learning problem and compare our method with the neural net based approaches.

Our experiments follow a similar setup to the previous problems; see Section B.5 for details. Once again the models were trained using data sets of size $I = 10$ or 20 and tested on a set of size 50 with forcing terms drawn from a GP. We also excluded the polynomial kernel as it was not competitive in this example. The results of our experiments with exact training data are summarized in Table 4 where our method with the ARD kernel achieved the lowest error followed closely by the large POD-DeepONet. Experimental

results with the noisy training set are presented in Table 2. Interestingly, in this setting large POD-DeepONet achieved the best errors followed very closely by our method (the difference is well within the standard deviation of the errors). In fact, the difference between our method, POD-DeepONet and FNO was quite small in this experiment compared to the previous two examples.

Method	10 sources	20 sources
$\mathcal{K} = \text{ARD}$	$1.4e^{-2}(1.5e^{-3})$	$7.1e^{-3}(1.0e^{-3})$
POD-DeepONet	$1.1e^{-1}(1.2e^{-2})$	$3.6e^{-2}(3.2e^{-3})$
POD-DeepONet (L)	$1.7e^{-2}(1.6e^{-3})$	$1.1e^{-2}(1.1e^{-3})$
FNO	$2.3e^{-1}(2.3e^{-2})$	$4.3e^{-2}(3.6e^{-3})$
DeepONet	$3.7e^{-1}(4.2e^{-2})$	$1.2e^{-1}(1.4e^{-2})$

Table 4. Average L^2 relative errors for the operator learning task of Darcy Flow computed for 50 test forcing functions. Standard deviations are reported in brackets. (L) indicates the large network variant of POD-DeepONet. Bold text indicates the best errors.

5. Discussion

Here we present a discussion regarding the various aspects of our method, how it compares to SINDy as well as neural net operator learning methods, and the implications of our experiments.

Main Takeaways From Experiments: Our experiments focused on the two distinct tasks of equation discovery and operator learning. Our results concerning equation discovery led to three primary observations: (a) kernel smoothing is a good pre-processing step for denoising and estimation of gradient information before learning DEs for both SINDy and our approach. In fact, our kernel method for Step (i) extends the applicability of SINDy to training data that is provided on unstructured meshes. (b) the performance of our method is closely tied to the choice of the kernel \mathcal{K} . With the polynomial kernel we matched the performance of SINDy in the pendulum and diffusion examples while the ARD kernel resulted in a local approximation to \mathcal{P} ; (c) Our kernel approach is more widely applicable than SINDy as demonstrated with the Darcy flow PDE where it is unclear how one could construct a dictionary for SINDy to begin with. Interestingly, here the ARD kernel appeared to yield good results while the polynomial kernel was far from being competitive.

Our results concerning operator learning led to two primary observations: (a) operator learning via PDE discovery consistently outperformed neural net based methods when exact training data was available (often by an order of magnitude). (b) the performance gap was smaller when noisy training data was involved but even then our method was (barely) beaten by the POD-DeepONet algorithm for the Darcy Flow example only. It is noteworthy that the POD-DeepONet was using a significantly larger set of parameters than our (much simpler) kernel method and it took significant tuning and ar-

chitecture adjustment to achieve this level of performance.

Our Abstract Framework: We highlight that our abstract three-step framework from Section 3 encompasses many existing equation discovery methods and extends them to perform operator learning. For example, choosing \mathcal{H} in Step (i) to be the appropriate RKHS associated to splines, we obtain the spline method implemented in the PySINDy package (de Silva et al., 2020) for estimating gradients. One can also take \mathcal{H} to be a Barron space (Ma et al., 2022) to obtain a neural net approximation for the derivatives. Choosing a sparsity promoting norm such as a 0-norm or a 1-norm (with $r = 1$) in Step (ii) yields the SINDy framework (Brunton et al., 2016) and its relatives while a Barron norm will once again yield a neural net approach such as PDE-Net (Long et al., 2018). The same is also true for Step (iii), one can choose \mathcal{H} to be a neural net space to obtain solvers such as PINNs (Raissi et al., 2019), or a discretized Sobolev space to obtain a classic finite element method, or an RKHS to obtain the approach of (Chen et al., 2021).

Discovering PDEs and the Role of Sparsity: The primary focus of the PDE/equation discovery literature (see for example (Bongard & Lipson, 2007; Schmidt & Lipson, 2009; Brunton et al., 2016; Schaeffer, 2017)) has been the extraction of explicit and interpretable equations that describe natural laws that govern physical processes. In our framework, this amounts to finding a simple and elegant expression for $\bar{\mathcal{P}}$. It is therefore natural to formulate Step (ii) over an appropriate set of features for $\bar{\mathcal{P}}$ and impose a sparsity assumption on those features, amounting to approaches such as SINDy. Our kernel approach on the other hand, does not aim to find a human interpretable expression for $\bar{\mathcal{P}}$ but rather approximates \mathcal{P} with a large number of features (possibly infinite) with the hope of achieving the best pointwise approximation error. Whether or not one chooses to employ the sparse dictionary/feature map approach or our kernel method, should be decided by downstream tasks that one wishes to perform with $\bar{\mathcal{P}}$. If we wish to discover a new interpretable natural law, then sparsity promoting methods are appropriate. If the goal is to perform operator learning, or if we are not confident in the quality of the dictionary, then the kernel method is more suitable.

Choosing Dictionaries and Learning kernels: It is well-known that the performance of sparsity promoting methods such as SINDy is closely tied to the construction of a good dictionary, in fact, in all of our experiments we used the dictionaries that were suggested by previous authors and were known to give competitive results. Put simply, if we have a good dictionary and the training data is sufficient, then we expect sparsity promoting methods to perform well. This fact has motivated various approaches, such as the Ensemble-SINDy (Fasel et al., 2022), that aim to automate and improve the construction of dictionaries. However, there

are various situations where the explicit construction of a dictionary is impossible. Consider our Darcy flow PDE (2) with a coefficient $a(x)$ that is unknown. In this case one cannot construct a simple dictionary of functions (such as polynomials) of the input variables to \mathcal{P} . This is of course possible if we knew the regularity of $a(x)$ and the manner in which \mathcal{P} depends on a but then we are injecting strong prior information into the problem.

Broadly speaking, the kernel approach, thanks to its large/infinite number of feature maps is more suitable in situations where very little information about the form of \mathcal{P} is available and variable coefficients exist. Another major advantage of the kernel approach is that it naturally accommodates the tuning/learning of kernel parameters which amounts to tailoring the feature maps to the problem at hand. This extra flexibility is what allowed us to obtain superior results in our operator learning experiments using CV.

Operator Learning via PDE Discovery vs Direct Regression: At the moment the dominant approach to operator learning in the literature can be broadly categorized as regression of maps between function spaces. Many existing algorithms such as DeepONets (Lu et al., 2021; 2022), FNOs (Li et al., 2020b; Anandkumar et al., 2020), the multipole graph neural operator (Li et al., 2020a), and the PCA-Net (Bhattacharya et al., 2021), fall within this category. Our approach to operator learning is fundamentally different from these methods as it relies on first learning the functional form of the PDE (that is \mathcal{P}), and then solving the learned PDE with a new forcing or boundary data. To our knowledge, our approach is the first of its kind and our experiments suggest that operator learning via PDE discovery is significantly more data efficient and gives superior performance. We conjecture this is due to the fact that our approach is tailored to PDEs and makes explicit use of our prior knowledge that the operator at hand is the solution map of a PDE, while the aforementioned techniques are more general.

6. CONCLUSION

An abstract three-step computational framework was presented for the discovery of DEs and operator learning of their solution maps via PDE discovery. A novel kernel implementation of this framework was presented and compared with state-of-the-art algorithms. Our experiments demonstrated that our method for equation discovery is competitively accurate and robust to noise while remaining applicable in broad such as PDEs with variable coefficients. For operator learning our method is significantly more data efficient when compared to general neural net methods that learn mappings between function spaces.

References

- Adams, R. A. and Fournier, J. J. *Sobolev spaces*. Elsevier, 2003.
- Anandkumar, A., Azizzadenesheli, K., Bhattacharya, K., Kovachki, N., Li, Z., Liu, B., and Stuart, A. Neural operator: Graph kernel network for partial differential equations. In *ICLR 2020 Workshop on Integration of Deep Neural Models and Differential Equations*, 2020.
- Battle, P., Chen, Y., Hosseini, B., Owhadi, H., and Stuart, A. M. Error analysis of kernel/GP methods for nonlinear and parametric PDEs. In preparation, 2023.
- Beck, J., Tempone, R., Nobile, F., and Tamellini, L. On the optimal polynomial approximation of stochastic pdes by galerkin and collocation methods. *Mathematical Models and Methods in Applied Sciences*, 22(09):1250023, 2012.
- Besginow, A. and Lange-Hegermann, M. Constraining gaussian processes to systems of linear ordinary differential equations. In *Advances in Neural Information Processing Systems*.
- Bhattacharya, K., Hosseini, B., Kovachki, N. B., and Stuart, A. M. Model reduction and neural networks for parametric pdes. *The SMAI journal of computational mathematics*, 7:121–157, 2021.
- Black, F. and Scholes, M. The pricing of options and corporate liabilities. *Journal of political economy*, 81(3):637–654, 1973.
- Bock, H. G. Numerical treatment of inverse problems in chemical reaction kinetics. In *Modelling of chemical reaction systems*, pp. 102–125. Springer, 1981.
- Bock, H. G. Recent advances in parameter identification techniques for ode. *Numerical treatment of inverse problems in differential and integral equations*, pp. 95–121, 1983.
- Bongard, J. and Lipson, H. Automated reverse engineering of nonlinear dynamical systems. *Proceedings of the National Academy of Sciences*, 104(24):9943–9948, 2007.
- Brunton, S. L., Proctor, J. L., and Kutz, J. N. Discovering governing equations from data by sparse identification of nonlinear dynamical systems. *Proceedings of the national academy of sciences*, 113(15):3932–3937, 2016.
- Carleo, G., Cirac, I., Cranmer, K., Daudet, L., Schuld, M., Tishby, N., Vogt-Maranto, L., and Zdeborová, L. Machine learning and the physical sciences. *Reviews of Modern Physics*, 91(4):045002, 2019.
- Chen, Y., Hosseini, B., Owhadi, H., and Stuart, A. M. Solving and learning nonlinear pdes with gaussian processes. *Journal of Computational Physics*, 447:110668, 2021.
- Chkifa, A., Cohen, A., DeVore, R., and Schwab, C. Sparse adaptive taylor approximation algorithms for parametric and stochastic elliptic PDEs. *ESAIM: Mathematical Modelling and Numerical Analysis*, 47(1):253–280, 2012.
- Chkifa, A., Cohen, A., and Schwab, C. High-dimensional adaptive sparse polynomial interpolation and applications to parametric pdes. *Foundations of Computational Mathematics*, 14(4):601–633, 2014.
- Cohen, A. and DeVore, R. Approximation of high-dimensional parametric pdes. *Acta Numerica*, 24:1–159, 2015.
- de Silva, B. M., Champion, K., Quade, M., Loiseau, J.-C., Kutz, J. N., and Brunton, S. L. Pysindy: a python package for the sparse identification of nonlinear dynamics from data. *arXiv preprint arXiv:2004.08424*, 2020.
- Edelstein-Keshet, L. *Mathematical models in biology*. SIAM, 2005.
- Fasel, U., Kutz, J. N., Brunton, B. W., and Brunton, S. L. Ensemble-sindy: Robust sparse model discovery in the low-data, high-noise limit, with active learning and control. *Proceedings of the Royal Society A*, 478(2260):20210904, 2022.
- Genton, M. G. Classes of kernels for machine learning: a statistics perspective. *Journal of machine learning research*, 2(Dec):299–312, 2001.
- Ghanem, R. G. and Spanos, P. D. *Stochastic finite elements: a spectral approach*. Dover Publications, 2003.
- Gulian, M., Frankel, A., and Swiler, L. Gaussian process regression constrained by boundary value problems. *Computer Methods in Applied Mechanics and Engineering*, 388:114117, 2022.
- Gunzburger, M. D., Webster, C. G., and Zhang, G. Stochastic finite element methods for partial differential equations with random input data. *Acta Numerica*, 23:521–650, 2014.
- He, Y., Suh, N., Huo, X., Kang, S. H., and Mei, Y. Asymptotic theory of-regularized pde identification from a single noisy trajectory. *SIAM/ASA Journal on Uncertainty Quantification*, 10(3):1012–1036, 2022a.
- He, Y., Zhao, H., and Zhong, Y. How much can one learn a partial differential equation from its solution? *arXiv preprint arXiv:2204.04602*, 2022b.
- Hesthaven, J. S., Rozza, G., Stamm, B., et al. *Certified reduced basis methods for parametrized partial differential equations*, volume 590. Springer, 2016.

- Hosseini, B., Jalalian, Y., Osorio Ramirez, J. F., and Owhadi, H. Error analysis of kernel equation learning via computational graph completion. In preparation, 2023.
- Jidling, C., Wahlström, N., Wills, A., and Schön, T. B. Linearly constrained gaussian processes. *Advances in Neural Information Processing Systems*, 30, 2017.
- Kaipio, J. and Somersalo, E. *Statistical and computational inverse problems*, volume 160. Springer Science & Business Media, 2006.
- Kang, S. H., Liao, W., and Liu, Y. Ident: Identifying differential equations with numerical time evolution. *Journal of Scientific Computing*, 87(1):1–27, 2021.
- Karniadakis, G. E., Kevrekidis, I. G., Lu, L., Perdikaris, P., Wang, S., and Yang, L. Physics-informed machine learning. *Nature Reviews Physics*, 3(6):422–440, 2021.
- Krämer, N., Bosch, N., Schmidt, J., and Hennig, P. Probabilistic ode solutions in millions of dimensions. In *International Conference on Machine Learning*, pp. 11634–11649. PMLR, 2022.
- Li, Z., Kovachki, N., Aizzadenesheli, K., Liu, B., Stuart, A., Bhattacharya, K., and Anandkumar, A. Multipole graph neural operator for parametric partial differential equations. *Advances in Neural Information Processing Systems*, 33:6755–6766, 2020a.
- Li, Z., Kovachki, N. B., Aizzadenesheli, K., Bhattacharya, K., Stuart, A., Anandkumar, A., et al. Fourier neural operator for parametric partial differential equations. In *International Conference on Learning Representations*, 2020b.
- Long, Z., Lu, Y., Ma, X., and Dong, B. PDE-Net: Learning pdes from data. In *International Conference on Machine Learning*, pp. 3208–3216. PMLR, 2018.
- Long, Z., Lu, Y., and Dong, B. PDE-Net 2.0: Learning PDEs from data with a numeric-symbolic hybrid deep network. *Journal of Computational Physics*, 399:108925, 2019.
- Lu, L., Jin, P., Pang, G., Zhang, Z., and Karniadakis, G. E. Learning nonlinear operators via deepnet based on the universal approximation theorem of operators. *Nature Machine Intelligence*, 3(3):218–229, 2021.
- Lu, L., Meng, X., Cai, S., Mao, Z., Goswami, S., Zhang, Z., and Karniadakis, G. E. A comprehensive and fair comparison of two neural operators (with practical extensions) based on fair data. *Computer Methods in Applied Mechanics and Engineering*, 393:114778, 2022.
- Lucia, D. J., Beran, P. S., and Silva, W. A. Reduced-order modeling: new approaches for computational physics. *Progress in aerospace sciences*, 40(1-2):51–117, 2004.
- Ma, C., Wu, L., et al. The barron space and the flow-induced function spaces for neural network models. *Constructive Approximation*, 55(1):369–406, 2022.
- Marsden, J. E. and Hughes, T. J. *Mathematical foundations of elasticity*. Dover Books, 1994.
- Mou, C., Yang, X., and Zhou, C. Numerical methods for mean field games based on gaussian processes and fourier features. *Journal of Computational Physics*, 460:111188, 2022.
- Muandet, K., Fukumizu, K., Sriperumbudur, B., Schölkopf, B., et al. Kernel mean embedding of distributions: A review and beyond. *Foundations and Trends® in Machine Learning*, 10(1-2):1–141, 2017.
- Nobile, F., Tempone, R., and Webster, C. G. An anisotropic sparse grid stochastic collocation method for partial differential equations with random input data. *SIAM Journal on Numerical Analysis*, 46(5):2411–2442, 2008a.
- Nobile, F., Tempone, R., and Webster, C. G. A sparse grid stochastic collocation method for partial differential equations with random input data. *SIAM Journal on Numerical Analysis*, 46(5):2309–2345, 2008b.
- Owhadi, H. and Scovel, C. *Operator-Adapted Wavelets, Fast Solvers, and Numerical Homogenization: From a Game Theoretic Approach to Numerical Approximation and Algorithm Design*, volume 35. Cambridge University Press, 2019.
- Owhadi, H. and Yoo, G. R. Kernel flows: From learning kernels from data into the abyss. *Journal of Computational Physics*, 389:22–47, 2019.
- Owhadi, H., Scovel, C., and Yoo, G. R. *Kernel Mode Decomposition and the programming of kernels*. Springer, 2021.
- Raissi, M., Perdikaris, P., and Karniadakis, G. E. Machine learning of linear differential equations using gaussian processes. *Journal of Computational Physics*, 348:683–693, 2017.
- Raissi, M., Perdikaris, P., and Karniadakis. Physics-informed neural networks: A deep learning framework for solving forward and inverse problems involving nonlinear partial differential equations. *Journal of Computational physics*, 378:686–707, 2019.
- Riley, K. F., Hobson, M. P., and Bence, S. J. *Mathematical methods for physics and engineering*. Cambridge University Press, 1999.

- Rudy, S. H., Brunton, S. L., Proctor, J. L., and Kutz, J. N. Data-driven discovery of partial differential equations. *Science advances*, 3(4):e1602614, 2017.
- Schaeffer, H. Learning partial differential equations via data discovery and sparse optimization. *Proceedings of the Royal Society A: Mathematical, Physical and Engineering Sciences*, 473(2197):20160446, 2017.
- Schmidt, J., Krämer, N., and Hennig, P. A probabilistic state space model for joint inference from differential equations and data. *Advances in Neural Information Processing Systems*, 34:12374–12385, 2021.
- Schmidt, M. and Lipson, H. Distilling free-form natural laws from experimental data. *science*, 324(5923):81–85, 2009.
- Stuart, A. Inverse problems: a bayesian perspective. *Acta numerica*, 19:451–559, 2010.
- Temam, R. *Navier-Stokes equations: theory and numerical analysis*, volume 343. American Mathematical Society, 2001.
- Tröltzsch, F. *Optimal control of partial differential equations: theory, methods, and applications*, volume 112. American Mathematical Soc., 2010.
- Wendland, H. *Scattered data approximation*, volume 17. Cambridge university press, 2004.
- Willard, J., Jia, X., Xu, S., Steinbach, M., and Kumar, V. Integrating physics-based modeling with machine learning: A survey. *arXiv preprint arXiv:2003.04919*, 2020.
- Xiu, D. *Numerical Methods for Stochastic Computations: A Spectral Method Approach*. Princeton University Press, 2010.
- Zhang, S., Yang, X., Tindel, S., and Lin, G. Augmented gaussian random field: Theory and computation. *Discrete & Continuous Dynamical Systems-S*, 15(4):931, 2022.

Appendix

A. Review of Relevant Literature

Below we present a review of the relevant literature to our work focusing on discovering/learning of PDEs, Operator Learning, and PDE solvers that use GPs and Kernels.

A.1. Discovering PDEs

Identifying the parameters of a differential equation (DE) is a well-known inverse problem; see the works of (Bock, 1983; 1981) on parameter identification of ordinary differential equations (ODEs) as well as the book of (Kaipio

& Somersalo, 2006) and the article of (Stuart, 2010) for examples involving PDEs. Such problems are also encountered in optimal control of PDEs as outlined in the book of (Tröltzsch, 2010). However, these classic approaches operate under the assumption that the expression of the DE is known up to free parameters that need to be identified from experimental data. Indeed, the approach of (Chen et al., 2021) readily extends to solving such inverse problems.

Equation discovery/learning is a more recent problem attributed to (Bongard & Lipson, 2007; Schmidt & Lipson, 2009) who used symbolic regression to discover underlying physical laws from experimental data. Compared with the aforementioned inverse problems, the goal here is to discover the very form of the DE as well as its parameters from experimental data. DEs that describe real world physical systems involve only a few terms and often have simple expressions. Based on this philosophy, recent approaches to equation learning try to learn a DE (i.e., the function \mathcal{P} in our formulation) from a dictionary of possible terms/features along with a sparsity assumption to ensure only a few terms will be active. Perhaps the best known example of such an approach is the SINDy algorithm of (Brunton et al., 2016; Rudy et al., 2017). SINDy has been expanded in many directions ever since (see (de Silva et al., 2020) and references within) and other authors have considered similar approaches (Schaeffer, 2017; Kang et al., 2021). At a high level, the differences between these approaches are in the formulation of the symbolic regression problem and the implementation of a sparsity assumption on the features (L_1 , L_0 regularization or various thresholding methods) as well as how they deal with noise in the training data.

Compared to the feature map perspective of SINDy-type methods, our approach employs a kernel perspective towards learning \mathcal{P} . As a result, we give up the immediate interpretability of the learned function $\bar{\mathcal{P}}$ in favor of more features and a more convenient computational framework that is also able to deal with more general PDEs, such as those involving spatial or temporally varying parameters. Feature based methods often cannot deal with such problems since the construction of appropriate features may require prior knowledge of the general form of the variable coefficients. Our method can also be combined with the kernel mode decomposition approach of (Owhadi et al., 2021) to extract the dominant features in the learned function $\bar{\mathcal{P}}$, thereby making our approach more interpretable. Additionally, our method opens the door for analyzing the accuracy and robustness of the estimator $\bar{\mathcal{P}}$. Such theoretical questions have attracted attention very recently (He et al., 2022a;b) although many open questions remain. Another closely related approach to our framework is the PDE-Net of (Long et al., 2018; 2019) which, put simply, parameterizes $\bar{\mathcal{P}}$ via a convolutional neural network. In this sense the PDE-Net approach can also be cast within our three step

abstract framework by replacing the space \mathcal{H}' in Step(ii) with a neural network space, ex. a Barron space (Ma et al., 2022).

A.2. Operator Learning

Approximation or learning of the solution maps of PDEs is a vast area of research in applied mathematics and engineering. In the setting of stochastic and parametric PDEs, the goal is often to approximate the solution of a PDE as a function of a random or uncertain parameter. The well-established approach to such problems is to pick or find appropriate bases for the input parameter and the solution of the PDE and then construct a parametric, high-dimensional map, that transforms the input basis coefficients to the output coefficients. Well-established methods such as polynomial chaos, stochastic finite element methods, reduced basis methods, and reduced order models (Ghanem & Spanos, 2003; Xiu, 2010; Cohen & DeVore, 2015; Hesthaven et al., 2016; Lucia et al., 2004) fall within this category. A vast literature in applied mathematics exists on this subject and the theoretical analysis of these methods has been the subject of extensive research; see for example (Beck et al., 2012; Chkifa et al., 2012; 2014; Nobile et al., 2008b;a; Gunzburger et al., 2014). More recent neural net based methods such as DeepONets (Lu et al., 2021), and FNO (Li et al., 2020b; Bhattacharya et al., 2021; Anandkumar et al., 2020) also fall within the aforementioned category of methods where the main novelty appears to be the use of novel neural network architectures that are very flexible, expressive, and allow the algorithm to learn and adapt the bases that are selected for the input and outputs of the solution map.

In contrast to the aforementioned methods, our three-step framework takes a different path towards operator learning. First, we formulate a regression problem in Step (ii) that approximates the algebraic form of the PDE, which is a much easier problem than direct approximation of the solution map. We then approximately evaluate the solution map by solving an optimization problem that solves a "nearby" PDE. To this end, our method is making explicit use of the knowledge that the operator of interest is the solution map of a PDE. One can also unroll the steps of the optimization problems in steps (ii) and (iii) of our method to obtain a neural net architecture for operator learning but it is unclear if this direction will lead to a reasonable algorithm.

A.3. Solving PDEs with GPs and Kernel methods

Finally, we mention that the key to our operator learning framework is the existence of flexible, meshless, and general purpose nonlinear PDE solvers such as the kernel method of (Chen et al., 2021) or PINNs (Raissi et al., 2019) that allow us to "solve" PDEs of the form $\overline{\mathcal{P}}(u) = f$, which in general, are ill-defined and ill-posed. When our kernel

approach to Step (ii) is employed we may end up with a function $\overline{\mathcal{P}}$ that has infinitely many feature maps, then a finite difference or finite element discretization of the resulting PDE is impossible or at least very expensive. This issue persists if we use a method such as SINDy since, even if $\overline{\mathcal{P}}$ has few terms, it may still involve stiff or unstable terms that need specialized solvers even if the true PDE is well-behaved. The above mentioned solvers, especially the kernel method of (Chen et al., 2021), allow us to overcome this difficulty since the solution of the equation is naturally regularized via the RKHS norm penalty. We emphasize that this penalty only provides stability at this stage and does not guarantee that the computed solution is actually accurate.

We also note that the use of kernel methods and GPs for solving PDEs has been an active area of research over the last decade; see for example (Jidling et al., 2017; Schmidt et al., 2021; Gulian et al., 2022; Zhang et al., 2022; Krämer et al., 2022; Besginow & Lange-Hegermann). Although the overwhelming majority of the research in this direction appears to be focused on the case of linear DEs. Some notable exceptions are (Raissi et al., 2017; Chen et al., 2021; Mou et al., 2022).

B. Details of Experiments

Below we present additional details regarding our experiments in Section 4.

B.1. Common Setup

For the kernel PDE solver in Step (iii) we used the implementation of (Chen et al., 2021) (<https://github.com/yifanc96/NonLinPDEs-GPsolver>). For estimation of derivatives in our method and the training of DeepONets we used Jax. For FNO we used the code base provided by the authors in (Li et al., 2020b). The POD-DeepONet was implemented using Pytorch. We used Python to implement SINDy, with iterative thresholding, with NumPy for the least squares step.

For all three DEs we conducted the experiments with $I = 10$ and 20 pairs of solutions-sources (the $u^{(i)}, f^{(i)}$ pairs in Section 3) in the training set. In the $I = 20$ case we also conducted experiments with a noisy training set where a Gaussian noise of noise-to-signal ratio 0.1 was added to both the training solutions and the training sources. In all of these experiments we validated the models on the same test set of 50 solution-source pairs.

For solving the optimization problem (16) we used the Gaussian-Newton algorithm of (Chen et al., 2021) for the pendulum ODE and the Diffusion PDE with 50 iterations. In the case of the Darcy flow PDE we ran 4000 steps of LBFGS with step sizes of 0.2 and 0.5. For all of the kernel matrices involved in our implementation we used diagonal

nugget terms of the form λI , where $\lambda > 0$ is a constant and I is an identity matrix of the same size as the requisite kernel matrix; also see Section 3.2. The value of η was tuned for each experiment separately; see tables 5–7 for a summary of the chosen nuggets.

For the POD-DeepONet we set the number of bases to maximum and varied the number of hidden layers from 2 to 3, and the width from 256, 512, and 1024. We trained for 100000 epochs to ensure convergence. We also trained a large variant of the POD-DeepONet (denoted as POD-DeepONet (L)) in Tables 1–4, where we set the width of the network to 8192. We implemented FNO using the standard four layer architecture for the integral operators, and varied the width over 64, 128, and 256. We trained the model for 4000 epochs to make sure it had converged. Finally we implemented the standard DeepONet with 2 and 3 hidden layers and varied the width from 256, 512, and 1024 and trained for 100000 epochs. All of the above neural nets were trained using the the Adam optimizer. We also used different activation functions (GELU, Tanh, and ReLU) and varied the learning rates from $1e^{-3}$, $1e^{-4}$, and $1e^{-5}$. The results reported in the Tables 1–4 for each neural net method were the best test errors that were obtained by searching over the aforementioned set of architectures and hyperparameters.

B.2. The Kernels

Throughout our experiments we used three kernels in Steps (i)–(iii) of our framework. The Gaussian kernel (also known as the squared exponential kernel)

$$\mathcal{K}_{\text{Gauss}}(\mathbf{t}, \mathbf{t}') = \exp\left(-\frac{\|\mathbf{t} - \mathbf{t}'\|^2}{2\sigma^2}\right) \quad \mathbf{t} \in \mathbb{R}^D,$$

with hyper-parameter $\sigma > 0$. We primarily used this kernel in Step (i) of all of our experiments for smoothing the training solutions $u^{(i)}$ and estimating their requisite partial derivatives. The same kernel was also used in Step (iii) and during the implementation of the kernel solver of (Chen et al., 2021).

We also considered a tensorized version of this kernel, which we referred to as the (automatic relevance determination) ARD kernel in our experiments:

$$\mathcal{K}_{\text{ARD}}(\mathbf{t}, \mathbf{t}') = \prod_{j=1}^D \exp\left(-\frac{|t_j - t'_j|^2}{2\ell_j^2}\right) \quad \mathbf{t} \in \mathbb{R}^D,$$

with hyper-parameters $\ell_1, \dots, \ell_D > 0$. The ARD kernel is simply a tensorization of 1D Gaussian kernels which uses a different length scale along each input coordinate. Finally, we also used the polynomial kernel

$$\mathcal{K}_{\text{Poly}}(\mathbf{t}, \mathbf{t}') = (\mathbf{t}^T \mathbf{t}' + c)^d, \quad \mathbf{t} \in \mathbb{R}^D,$$

with hyper-parameters $c > 0$ and $d \in \mathbb{N}$. We only considered $d = 2, 3, 4$, and 5. For all experiments we used cross

validation to choose the hyperparameters. The ARD and polynomial kernels were used in Step (ii) of our framework.

B.3. Pendulum

The training data was generated by the following recipe: the source terms $f^{(i)}$ for $i = 1, \dots, I$ were drawn independently from a GP with the RBF kernel and lengthscale 0.2. For each source term the ODE was solved using the SciPy solve_ivp function on a fine grid and sub-sampled over a uniform grid of the t_j 's for $j = 1, \dots, 30$. The test data was generated using the same recipe except that 50 independent source terms were drawn. For operator learning the L^2 errors between the predicted solutions and the test solutions were computed over the t_j grid and then averaged over the test set, the values reported in Tables 1–4. When implementing SINDy, we implemented the first equation exactly and only learned the second equation using the dictionary $\{(u_2)_t(t), u_1(t), u_1(t)^2, u_1(t)^3, \sin(u_1(t)), \cos(u_1(t)), 1\}$.

When implementing our method we learned each equation in the system separately assuming that the right hand side for each coordinate is a function of both u_1 and u_2 , i.e., we considered the system of ODEs

$$\begin{aligned} (u_1)_t(t) &= \overline{\mathcal{P}}_1(u_1(t), u_2(t)) \\ (u_2)_t(t) &= \overline{\mathcal{P}}_2(u_1(t), u_2(t)). \end{aligned}$$

All hyperparameters involved in the training of our kernel method for this example are summarized in Table 5. We used the Gaussian kernel for Step (i) but length scales were tuned for each instance of the data separately, therefore we report only the range of σ for each coordinate of the solution. The Gaussian kernel was also used for Step (iii) with a lengthscale that was chosen in the same range that was tuned for Step (i). We also used different lengthscales for each of $\overline{\mathcal{P}}_1$ and $\overline{\mathcal{P}}_2$ as indicated in the table.

Hyper-parameters $I = 10$ $I = 20$ $I = 20$ (Noisy)				
(i):	$\lambda_{\mathcal{U}}$	$1.0e^{-8}$	$1.0e^{-8}$	$1.0e^{-8}$
u_1	σ	(0.15, 0.45)	(0.15, 0.65)	
u_2	σ	(0.1, 0.4)	(0.1, 0.8)	
(ii):	$\lambda_{\mathcal{C}}$	$1.0e^{-5}$	$1.0e^{-5}$	$1.0e^{-1}$
$\overline{\mathcal{P}}_1$	$\ell_1 = \ell_2$	0.52	1.0	1.0
	d	5	3	1
	c	3.5	0.015	0.01
$\overline{\mathcal{P}}_2$	$\ell_1 = \ell_2$	3.0	2.4	1.9
	d	5	3	1
	c	2.8	0.01	0.01

Table 5. The hyper-parameters we used for the pendulum experiments for exact training sets of size $I = 10, 20$ as well as the noisy training set of size $I = 20$.

B.4. Diffusion PDE

The test data set was generated by drawing the source terms from the same GP as in the pendulum example of Section B.3. The solution $u^{(i)}(x, t)$ for each force $f^{(i)}(x)$ was

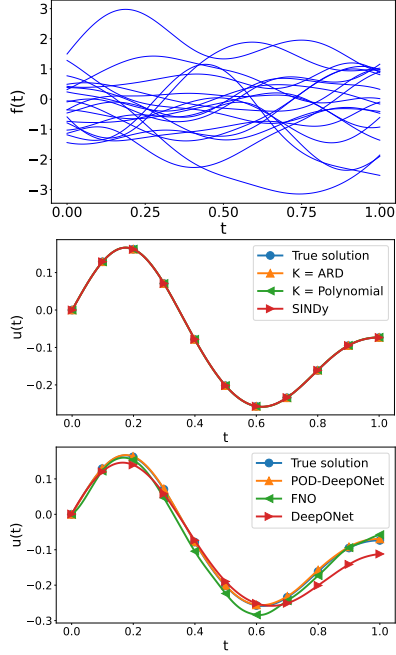


Figure 2. (Top) the forcing terms used to generate the training data for the pendulum ODE. (Middle) comparing the ODE solutions obtained from our model and SINDy for one of the test forcing terms. (Bottom) comparing the ODE solutions obtained from POD-DeepONet, FNO, and DeepONet for one of the test forcing terms. Results were obtained with training set of size 20.

computed on a fine grid using an independent finite difference solver before they were subsampled to a space-time grid of size 15×15 , constituting the training set, so for each tuple $(u^{(i)}, f^{(i)})$ we collected a total of 225 values for a total training set size of $I = 10$ and 20. The test data set was produced in the same manner for 50 pairs of solutions and sources. The errors were once again computed by averaging the L^2 errors over the test set. When implementing SINDy we used the dictionary of functions $\{u_t, u_{xx}, u, u^2, u^3, u \cdot u_{xx}, u^2 \cdot u_{xx}, u^3 \cdot u_{xx}, u \cdot u_t, u^2 \cdot u_t, u^3 \cdot u_t, 1\}$.

We parameterized the PDE as

$$\overline{\mathcal{P}}(u(x, t), u_t, u_{xx}(x, t)) = f(x).$$

All hyperparameters involved in the training of our kernel method for this example are summarized in Table 6. Once again we used the Gaussian kernel for Step (i) while the ARD and polynomial kernels were used for Step (ii). Step (iii) also used the Gaussian kernel with a lenscale that was chosen in the same range that was found in Step (i). We also present an example of the predicted solutions of the PDE from the test set in Figure 3.

Hyper-parameters	$I = 10$	$I = 20$	$I = 20$ (Noisy)
(i): $\lambda_{\mathcal{U}}$	$1.0e^{-3}$	$1.0e^{-3}$	$1.0e^{-3}$
σ	(0.15, 0.7)		(0.4, 1.0)
(ii): $\lambda_{\mathcal{K}}$	$1.0e^{-3}$	$1.0e^{-3}$	$1.0e^{-3}$
(ℓ_1, \dots, ℓ_3)	(0.50, 1.3, 0.13)	(0.50, 1.3, 0.13)	(0.50, 2.0, 0.25)
d	2	2	Failed
c	0.23	0.0	Failed

Table 6. The hyper-parameters we used for the diffusion experiment for exact training sets of size $I = 10, 20$ as well as the noisy training set of size $I = 20$. Reported "Failed" values indicate high errors that were not competitive.

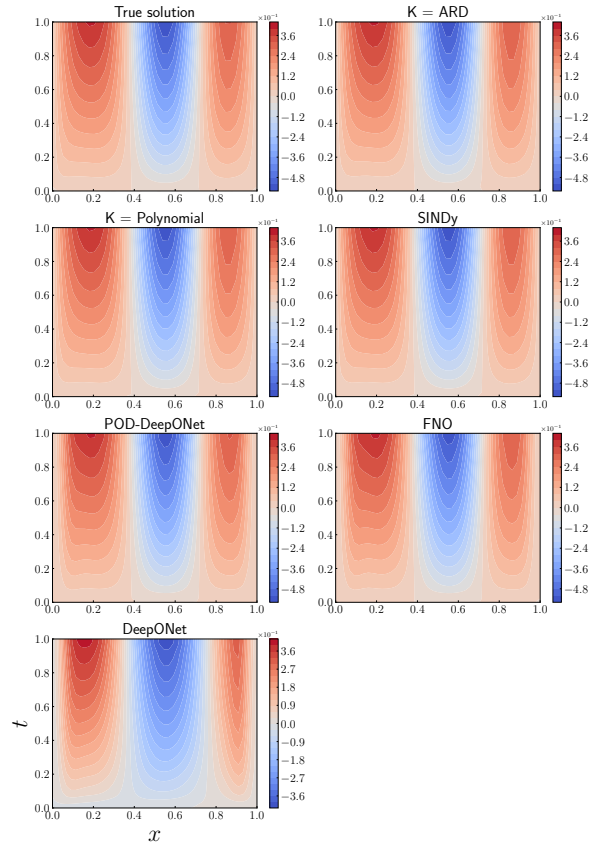


Figure 3. A comparison of the estimated solutions to the diffusion PDE for one of the forcing terms in the test set with training set of size $I = 20$.

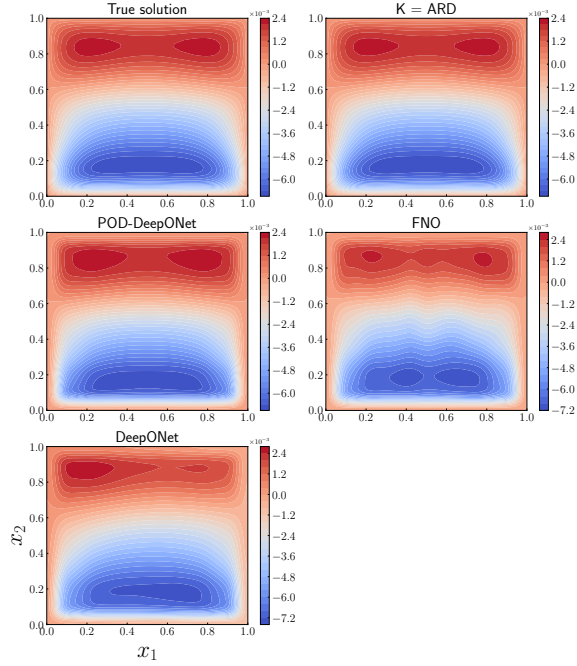


Figure 4. A comparison of the estimated solutions to the Darcy flow PDE for one of the forcing terms in the test set (the 20 training source experiment).

B.5. Darcy Flow

The training and test sources for the Darcy flow PDE were generated by taking $f(x_1, x_2) \equiv f(x_2)$ and drawing this function from a 1D GP with the RBF kernel and length scale 0.2. The PDE was then solved using a finite difference solver, on a fine mesh and the solutions were subsampled to a uniform grid of size 15×15 , following a similar scheme to the diffusion PDE. The test set was generated in the same manner.

We parameterized the PDE as

$$\overline{\mathcal{P}}(x_1, x_2, u, u_{x_1}, u_{x_2}, \Delta u) = f(\mathbf{x}).$$

All hyperparameters involved in the training of our kernel method for this example as summarized in Table 7. The Gaussian kernel was used for Step (i) while the ARD kernel was used for Step (ii). Our experiments using the polynomial kernel for this step lead to bad results. Step (iii) also used the Gaussian kernel with a lengthscale that was chosen in the range that was tuned in Step (i). Example solutions from the test set are presented in Figure 4.

Hyper-parameters	$I = 10$	$I = 20$	$I = 20$ (Noisy)
(i): $\lambda_{\mathcal{L}}$	$1.0e^{-8}$	$1.0e^{-8}$	$1.0e^{-2}$
σ	(0.15, 0.35)		(0.05, 0.5)
(ii): $\lambda_{\mathcal{K}}$	$1.0e^{-3}$	$1.0e^{-3}$	$1.0e^{-1}$
(ℓ_1, \dots, ℓ_6)	(1.2, 1.2, 8.0, 8.0, 10.0, 10.0)	(0.4, 0.4, 3.2, 3.2, 5.0, 5.0)	(0.64, 0.64, 2.0, 2.0, 3.0, 3.0)

Table 7. The hyperparameters we used for the Darcy Flow experiments for exact training sets of size $I = 10, 20$ as well as noisy training set of size $I = 20$.